Nonlinear Analysis: Modelling and Control, Vol. 21, No. 5, 587–599 ISSN 1392-5113
http://dx.doi.org/10.15388/NA.2016.5.2

Unified linear time-invariant model predictive control for strong nonlinear chaotic systems*

Yuan Zhang, Mingwei Sun, Zengqiang Chen

College of Computer and Control Engineering, Nankai University
Tianjin, 300350, China
nankaizhangyuan@163.com; smw_sunmingwei@163.com; chenzq@nankai.edu.cn

Received: December 2, 2014 / **Revised:** October 19, 2015 / **Published online:** June 23, 2016

Abstract. It is well known that an alone linear controller is difficult to control a chaotic system, because intensive nonlinearities exist in such system. Meanwhile, depending closely on a precise mathematical modeling of the system and high computational complexity, model predictive control has its inherent drawback in controlling nonlinear systems. In this paper, a unified linear time-invariant model predictive control for intensive nonlinear chaotic systems is presented. The presented model predictive control algorithm is based on an extended state observer, and the precise mathematical modeling is not required. Through this method, not only the required coefficient matrix of impulse response can be derived analytically, but also the future output prediction is explicitly calculated by only using the current output sample. Therefore, the computational complexity can be reduced sufficiently. The merits of this method include, the Diophantine equation needing no calculation, and independence of precise mathematical modeling. According to the variation of the cost function, the order of the controller can be reduced, and the system stability is enhanced. Finally, numerical simulations of three kinds of chaotic systems confirm the effectiveness of the proposed method.

Keywords: chaos, extended state observer, predictive control, synchronization.

1 Introduction

Chaos is one of the important properties for some nonlinear systems, which show bounded instability. A chaotic system has several remarkable characteristics, for instance, positive Lyapunov exponent, aperiodic trajectory, sensitivity to initial conditions, unpredictability of long-range behavior and ergodicity [24]. Along with the invention of several novel chaotic systems [9, 28], chaos control and synchronization have also been extensively investigated since the pioneering OGY method [14] was proposed. In this field, many schemes, including delayed feedback control [2, 4, 15], backstepping control [21], fuzzy

*This work was supported in part by the Natural Science Foundation of China (grant Nos. 61174094, 61273138 and 61573197) and the Tianjin Natural Science Foundation (grant Nos. 14JCYBJC18700 and 13JCYBJC17400).

control [5, 12, 25], adaptive control [18, 22], neural network control [8, 19], sliding mode control [20, 26, 27], etc., have already been employed. Note that all these methods are nonlinear. Generally, nonlinear control methods have played dominant role in controlling chaotic systems because of their nonlinear nature. Few completely linear control approaches were also utilized to control chaos [13]. The core philosophy of [13] is to eliminate the original nonlinear dynamics by using observer. This strategy is effective in many industrial applications [29, 30]. Therefore, it is possible to control an intensive nonlinear system by using a linear time-invariant controller, providing that an appealing alternative in practice wherein simple control mechanisms are always sought.

Model predictive control (MPC) is an important option for industrial applications in recent years. Generalized predictive control (GPC) [3], which was combined with identification and self-tuning algorithm, was proposed in 1987. GPC can be used to control a wide range of complicated systems with non-minimum-phase, open-loop unstable and time-delay characteristics. GPC was also utilized to control chaos [11], however there are two controversial issues: firstly, traditional MPC is closely dependent on precise system modeling, and this method exhibits an intrinsic drawback of insufficient robustness to model uncertainties; secondly, the high computational complexity caused by output prediction or parameter identification is intolerable in many scenarios. For the intensive nonlinear chaotic system, these calculation procedures are more burdensome. Therefore, a simple and effective MPC approach is required to handle such sophisticated chaotic nonlinear systems.

In this paper, a unified linear time-invariant (LTI) MPC independent of system modeling is proposed to control the chaos. An extended state observer (ESO) [7] is adopted to transform the chaotic system into an approximate integrator, which serves as the predictive model. Then GPC can be designed for the integrator such that the characteristic parameters of the chaotic systems are not necessary. On the other hand, the Diophantine equations are not required, and the future output predictions can be explicitly calculated. Generally, this method is a unified manner to achieve control and synchronization of chaotic systems.

This paper is organized as follows. Section 2 presents the linearization procedure for a chaotic system via ESO. Section 3 gives the design of a unified LTI MPC with further simplifications. The simulation results are provided in Section 4. Section 5 summarizes the concluding remarks.

2 Linearization of chaos with dynamic compensation

The dynamic model of a n-dimensional chaotic system can be described as follows:

$$\dot{X} = F(X), \tag{1}$$

where $X = [x_1, x_2, \ldots, x_n]^{\mathrm{T}}$ is the state vector, $F = [f_1, f_2, \ldots, f_n]^{\mathrm{T}}$ is a function vector, and f_i $(i = 1, 2, \ldots, n)$ are continuous functions. Assume that the number of states that can be controlled directly is m $(m \leqslant n)$, and their subscripts are $r_1, r_2, \ldots, r_m$,

respectively. Then, the controllable subsystem can be written as

$$\dot{x}_{r_k} = f_{r_k}(X) + u_{r_k}, \tag{2}$$

where u_{r_k} is the corresponding control input. The state-space form of each controllable subsystem can be represented as

$$\begin{aligned} \dot{x}_{k,1} &= x_{k,2} + u_{r_k}, \\ \dot{x}_{k,2} &= \dot{f}_{r_k}(X), \\ y_{r_k} &= x_{k,1}, \end{aligned} \tag{3}$$

where $x_{k,1} = x_{r_k}$ and $x_{k,2} = f_{r_k}(X)$. Here, $x_{k,2}$ is defined as an extended state [7]. It should be noted that this innovative extended state is just an intermediate signal rather than a practical state, and it has no physical meaning. For model-based control approaches, for instance, the well-known pole-placement method for linear time-invariant systems and the feedback linearization method for nonlinear systems, it is assumed that the analytical expression of $x_{k,2}$ sufficiently approaches to its corresponding part in physical reality. Specifically, $x_{k,2}$ is generally nonlinear and time-varying. In fact, when this model-based approach was put into practice, it was often found that the engineers spent much time on modeling rather than on controller design. The advantage of the extended state is that it treats $x_{k,2}$ as a whole without any distinction of its originality. In modern control theory, the state observer is used in the full-state feedback strategy when not all states are measurable. A full-order state observer for (3) is designed as

$$\begin{aligned} \dot{z}_{k,1} &= z_{k,2} + l_1(y_{r_k} - \hat{y}_{r_k}) + u_{r_k}, \\ \dot{z}_{k,2} &= l_2(y_{r_k} - \hat{y}_{r_k}), \\ \hat{y}_{r_k} &= z_{k,1}. \end{aligned} \tag{4}$$

Moreover, to simplify the tuning process, the observer gains l_1, l_2 can be parameterized as a bandwidth ω_o

$$[l_1, l_2] = \left[2\omega_o, \omega_o^2\right]. \tag{5}$$

In (4), the second state $z_{k,2}$ approximates to the nonlinear dynamics of controllable subsystem, or to the extended state $x_{k,2}$, which will be used in the subsequent control design. Because of the linear observer gains, this observer is called as the linear extended state observer (LESO) [6].

There is a redundancy for the full-order LESO since $x_{k,1}$ can be measured directly. To reduce complexity and the phase lag, a reduced-order LESO [16, 23] can be designed for $x_{k,2}$. According to (3), one has

$$\begin{aligned} \dot{x}_{k,2} &= \dot{f}_{r_k}(X), \\ y'_{r_k} &= x_{k,2}, \end{aligned} \tag{6}$$

where the new measurement variable y'_{r_k} can be expressed as

$$y'_{r_k} = \dot{x}_{k,1} - u_{r_k}. \tag{7}$$

In terms of (6) and (7), the observer for $x_{k,2}$ can be written as

$$\dot{z}'_{k,2} = \omega_o(-u_{r_k} - z'_{k,2} + \dot{x}_{k,1}). \tag{8}$$

Because $\dot{x}_{k,1}$ is not available, a new state is defined as

$$z'_{k,c} = z'_{k,2} - \omega_o x_{k,1}, \tag{9}$$

which can yield a linear reduced-order state observer for (3), i.e.,

$$\dot{z}'_{k,c} = -\omega_o z'_{k,2} - \omega_o u_{r_k}. \tag{10}$$

With a well-tuned observer bandwidth, an estimate is obtained as $z'_{k,2} \approx x_{k,2} = f_{r_k}(X)$. Hence, we can design u_{r_k} as

$$u_{r_k} = u_{0,k} - z'_{k,2}, \tag{11}$$

where $u_{0,k}$ is a virtual control variable. Therefore, the original plant (2) can be transformed into an integrator, i.e.,

$$\dot{x}_{r_k} \approx u_{0,k}. \tag{12}$$

In the process, the characteristic parameters of chaotic system are not required any more, so the dependence on the precise modeling can be ignored. This ESO is linear time-invariant but its design concept is totally different: it applies to nonlinear, time varying, uncertain process with very little model information. Thus, The MPC design can be performed for the simple integrator while the nonlinear dynamics vanishes. This offers a possibility to enhance the robustness of MPC considerably.

3 The unified LTI MPC for chaos

As mentioned above, the chaotic system can be reformulated as an integrator with feedback linearization by using ESO. Then, the unified LTI GPC independent of nonlinear dynamic model can be implemented for this integrator. The block diagram is shown in Fig. 1.

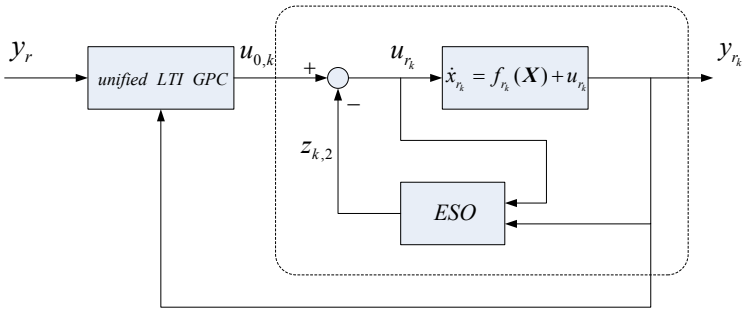

Figure 1. Block diagram of the proposed scheme.

The discrete-time form of the integrator (12) is

$$\frac{x_{r_k}(z^{-1})}{u_{0,k}(z^{-1})} \approx z^{-1}\frac{B(z^{-1})}{A(z^{-1})}, \tag{13}$$

where $A(z^{-1}) = 1 - z^{-1}$, $B(z^{-1}) = h$, h is the sampling time. The cost function is

$$J = \sum_{j=1}^{N}\left[\hat{y}_{r_k}(k+j \mid k) - y_{r_k-d}(k+j)\right]^2 + \lambda\sum_{j=1}^{N_u}\left[u_{0,k}(k+j-1)\right]^2. \tag{14}$$

Here λ ($\lambda > 0$) is a weight coefficient on control variable, N and N_u are the predictive horizon and the control horizon, and when $j > N_u$, the following relation holds:

$$u_{0,k}(k+j-1) = 0. \tag{15}$$

$\hat{y}_{r_k}(k+j\,|\,k)$ is the future output prediction at time $k+j$ according to the known information at the current instant k, and $y_{r_{k-d}}(k+j)$ is a reference, which is given by

$$\begin{aligned} &y_{r_k-d}(k) = y_{r_k}(k),\\ &y_{r_k-d}(k+j) = \alpha y_{r_k-d}(k+j-1) + (1-\alpha)y_r(k), \end{aligned} \tag{16}$$

where $y_r(k)$ is the current set-point, and α ($0 \leqslant \alpha \leqslant 1$) is a smoothing factor. It is noted that, due to the existence of an integrator in (13) after ESO compensation, the absolute value of control action instead of its increment as done in [3] is penalized. The order of the controller can be reduced such that the system stability can be enhanced.

Theorem 1. *When all the future virtual controls are zero, the future output predictions are independent of the input, that is* $\hat{y}_{r_k}(k+j \mid k) = y_{r_k}(k)$, $j = 1, 2, \ldots, N$.

Proof of Theorem 1. In order to obtain the jth step-ahead output prediction, consider the Diophantine equation as

$$1 = E_j\big(z^{-1}\big)A\big(z^{-1}\big) + z^{-j}F_j\big(z^{-1}\big), \tag{17}$$

where E_j, F_j are the polynomials in terms of z^{-1}, i.e.,

$$\begin{aligned} &E_j\big(z^{-1}\big) = e_0 + e_1 z^{-1} + \cdots + e_{j-1}z^{-(j-1)},\\ &F_j\big(z^{-1}\big) = f_{j0}. \end{aligned} \tag{18}$$

Because the forms of $A(z^{-1})$ and $B(z^{-1})$ are simple, the solution of (18) can be readily obtained by employing mathematical induction method as follows:

$$\begin{aligned} &E_j\big(z^{-1}\big) = 1 + z^{-1} + \cdots + z^{-(j-1)},\\ &F_j\big(z^{-1}\big) = 1. \end{aligned} \tag{19}$$

Premultiplying (17) by $B(z^{-1})$ gives

$$B\big(z^{-1}\big) = B\big(z^{-1}\big)E_j\big(z^{-1}\big)A\big(z^{-1}\big) + B\big(z^{-}1\big)z^{-j}F_j\big(z^{-1}\big) \tag{20}$$

and

$$B\big(z^{-1}\big)E_j\big(z^{-1}\big) = G_j\big(z^{-1}\big) + z^{-j}H_j\big(z^{-1}\big), \tag{21}$$

where the orders of G_j and H_j are, respectively,

$$\begin{aligned} &\deg\big(G_j\big(z^{-1}\big)\big) = j-1,\\ &\deg\big(H_j\big(z^{-1}\big)\big) = 0. \end{aligned} \tag{22}$$

By using (20) and (21), G_j can be expressed as

$$G_j\big(z^{-1}\big) = \frac{B(z^{-1})}{A(z^{-1})}. \tag{23}$$

Hence, the coefficients of $G_j(z^{-1})$ are just the first j terms of the impulse response for the plant (13), and

$$G_j\big(z^{-1}\big) = h + hz^{-1} + \cdots + hz^{-(j-1)}. \tag{24}$$

Combining (21), (22) and (24) leads to

$$H_j\big(z^{-1}\big) = 0. \tag{25}$$

Consequently, the future output prediction can be written as

$$\begin{aligned} &\hat{y}_{r_k}(k+j \mid k)\\ &\quad = G_j\big(z^{-1}\big)u_{0,k}(k+j-1) + F_j\big(z^{-1}\big)y_{r_k}(k) + H_j\big(z^{-1}\big)u_{0,k}(k-1)\\ &\quad = G_j\big(z^{-1}\big)u_{0,k}(k+j-1) + F_j\big(z^{-1}\big)y_{r_k}(k). \end{aligned} \tag{26}$$

In case of $\{u_{0,k}(k+j-1),\ j=1,2,\ldots,N\}$ being zero, (26) becomes

$$\hat{y}_{r_k}(k+j \mid k) = F_j\big(z^{-1}\big)y_{r_k}(k) = y_{r_k}(k), \quad j=1,2,\ldots,N. \tag{27}$$

This concludes the proof. □

In addition, the coefficient matrix G of impulse response can be directly expressed as

$$G(i,j)_{N\times N_u} = \begin{cases} h, & i \geqslant j,\\ 0, & i < j, \end{cases} \tag{28}$$

and

$$G^{\mathrm{T}}G(i,j) = h^2\big(N - \big(\max(i,j)-1\big)\big). \tag{29}$$

In order to optimize the cost function, the optimal prediction $\hat{y}_{r_k}(k+j \mid k)$ can be reformulated as

$$\hat{Y}_{r_k}(k) = \hat{Y}_{r_{k-0}}(k) + GU_{0,k}(k). \tag{30}$$

where

$$\hat{Y}_{r_k}(k) = \big[\hat{y}_{r_k}(k+1 \mid k),\ \hat{y}_{r_k}(k+2 \mid k),\ \ldots,\ \hat{y}_{r_k}(k+N \mid k)\big]^{\mathrm{T}}, \tag{31}$$

$$\hat{Y}_{r_k-0}(k) = \big[\hat{y}_{r_k-0}(k+1 \mid k),\ \hat{y}_{r_k-0}(k+2 \mid k),\ \ldots,\ \hat{y}_{r_k-0}(k+N \mid k)\big]^{\mathrm{T}}, \tag{32}$$

$$Y_{r_k-d}(k) = = \big[y_{r_k-d}(k+1),\ y_{r_k-d}(k+2),\ \ldots,\ y_{r_k-d}(k+N)\big]^{\mathrm{T}}, \tag{33}$$

$$U_{0,k}(k) = \big[u_{0,k}(k),\ u_{0,k}(k+1),\ \ldots,\ u_{0,k}(k+N_u-1)\big]^{\mathrm{T}}. \tag{34}$$

Here $\hat{Y}_{r_k-0}(k)$ is the zero input response component, and $GU_{0,k}(k)$ is the zero state response one. Then the cost function can be rewritten as

$$\begin{aligned} J = {} & \big[\hat{Y}_{r_{k-0}}(k) + GU_{0,k}(k) - Y_{r_{k-d}}(k)\big]^{\mathrm{T}}\big[\hat{Y}_{r_{k-0}}(k) + GU_{0,k}(k) - Y_{r_{k-d}}(k)\big] \\ & + \lambda\big[U_{0,k}(k)\big]^{\mathrm{T}}\big[U_{0,k}(k)\big]. \end{aligned} \tag{35}$$

By letting

$$\frac{\partial J}{\partial U_{0,k}(k)} = 0, \tag{36}$$

one can obtain

$$U_{0,k}(k) = \big(G^{\mathrm{T}}G + \lambda I\big)^{-1}G^{\mathrm{T}}\big[Y_{r_k-d}(k) - \hat{Y}_{r_k-0}(k)\big], \tag{37}$$

and $u_{0,k}(k)$ is the first component of $U_{0,k}(k)$, i.e.,

$$\begin{aligned} u_{0,k}(k) &= [1,0,\ldots,0]\,U_{0,k}(k) \\ &= [1,0,\ldots,0]\big(G^{\mathrm{T}}G + \lambda I\big)^{-1}G^{\mathrm{T}}\big[Y_{r_k-d}(k) - Y_{r_k-0}(k)\big]. \end{aligned} \tag{38}$$

Only $u_{0,k}(k)$ is put into the operation. In the next sampling time interval, this procedure is repeated.

4 Simulation result

In this section, a continuous chaotic system and a switching chaotic system are adopted, respectively, to confirm the effectiveness of the proposed method.

4.1 Control of a continuous chaotic system

In [17], a novel continuous chaotic model was presented as

$$\begin{aligned} \dot{x} &= a(y-x) + yz, \\ \dot{y} &= bx - y - xz, \\ \dot{z} &= cy - dz + xy, \end{aligned} \tag{39}$$

where a, b, c, d are constants, and x, y, z are the state variables. When $a = 16$, $b = 50$, $c = 8$ and $d = 4$, the chaotic behavior is exhibited.

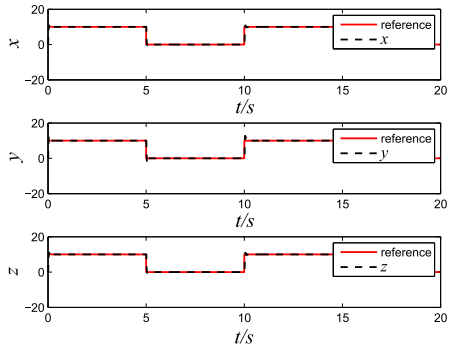

Figure 2. Responses of the three states.

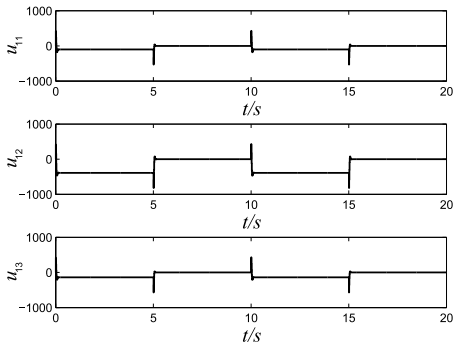

Figure 3. Control signals.

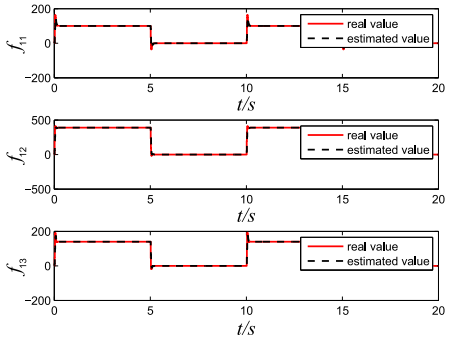

Figure 4. ESO estimations.

We select u_{11}, u_{12} and u_{13} to control the three states to track the square waves, respectively. The control parameters are identically selected as $N = 50$, $N_u = 2$, $\lambda = 0.001$, $\alpha = 0.1$, and $\omega_{o_{11}} = \omega_{o_{12}} = \omega_{o_{13}} = 50$. The sampling time interval is 10 ms.

The responses are shown in Figs. 2–4. It is shown that each state can track the reference signal exactly and the nonlinear dynamics can be captured rapidly by ESO.

4.2 Self-synchronization of a continuous chaotic system

The drive system is [17]

$$\begin{aligned} \dot{x}_1 &= a(y_1 - x_1) + y_1 z_1, \\ \dot{y}_1 &= bx_1 - y_1 - x_1 z_1, \\ \dot{z}_1 &= cy_1 - dz_1 + x_1 y_1, \end{aligned} \tag{40}$$

and the response system is

$$\begin{aligned} \dot{x}_2 &= a(y_2 - x_2) + y_2 z_2 + u_{21}, \\ \dot{y}_2 &= bx_2 - y_2 - x_2 z_2, \\ \dot{z}_2 &= cy_2 - dz_2 + x_2 y_2. \end{aligned} \tag{41}$$

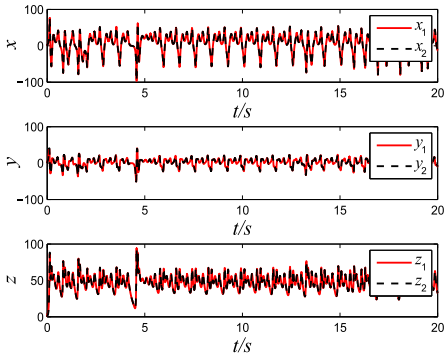

Figure 5. Time responses of the states.

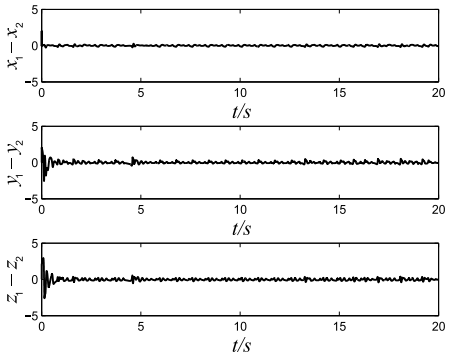

Figure 6. Synchronization errors.

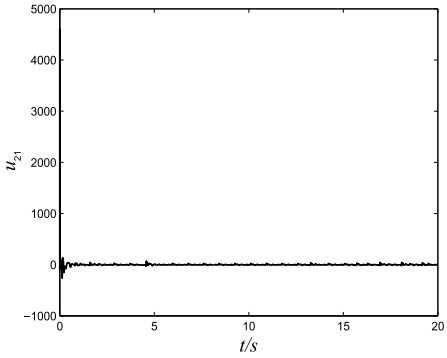

Figure 7. Control variable.

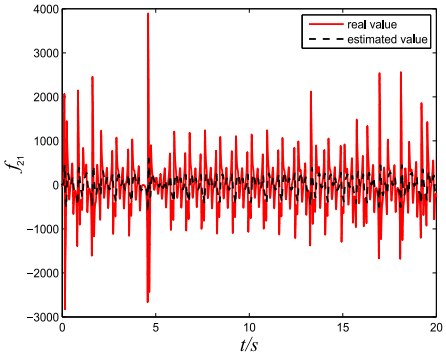

Figure 8. ESO estimation of f_{21}.

The constants are the same as those in the previous example. However, only the first state is controlled to achieve synchronization, which is different from the previous example. It is the unique property of the chaotic system that the global stability can be achieved by using less control variables due to the strong coupling among the states [1].

The initial conditions of the response system are $x_2(0) = 1$, $y_2(0) = 1$, $z_2(0) = 1$ and $u_{21}(0) = 0$ while the initial states of drive system are $x_1(0) = 3$, $y_1(0) = 3$ and $z_1(0) = 3$. We select $N = 200$, $N_u = 2$, $\lambda = 0.000001$, $\alpha = 0.1$, and $\omega_{o_{21}} = 8$. The sampling time interval is 0.2 ms. The responses are illustrated in Figs. 5–8. It is clear that although only one channel is controlled, the three channels are synchronized effectively.

4.3 Control of a switching chaotic system

The passive bipedal walking model [10], which is a kind of switching system, can be described as

$$\begin{aligned} \ddot{\theta} &= \sin(\theta - \gamma), \\ \ddot{\phi} &= \sin\phi\left[\dot{\theta}^2 - \cos(\theta - \gamma)\right] + \sin(\theta - \gamma), \end{aligned} \tag{42}$$

and the switching manifold is

$$\phi - 2\theta = 0. \tag{43}$$

When (43) is achieved at $(\theta^-,\ \phi^-,\ \dot{\theta}^-,\ \dot{\phi}^-)$, the system switches to

$$\begin{aligned} \theta^+ &= -\theta^-, \\ \phi^+ &= -2\theta^-, \\ \dot{\theta}^+ &= \cos(2\theta^-)\dot{\theta}^-, \\ \dot{\phi}^+ &= \cos(2\theta^-)\big(1-\cos(2\theta^-)\big)\dot{\theta}^-. \end{aligned} \tag{44}$$

The system is chaotic when $\gamma = 0.0129$ [10].

At first, equation (42) with control can be represented as

$$\begin{aligned} \dot{x}_{31} &= f_{31} + u_{31}, \\ \dot{x}_{32} &= f_{32} + u_{32}, \end{aligned} \tag{45}$$

where $x_{31} = \dot{\theta}$, $x_{32} = \dot{\phi}$; $f_{31} = \sin(\theta-\gamma)$ and $f_{32} = \sin\phi[x_{31}^2 - \cos(\theta-\gamma)] + \sin(\theta-\gamma)$ are extended states; u_{31} and u_{32} are the control variables to make θ and ϕ track the square wave $(\theta_r,\ \phi_r)$. The set-points of x_{31} and x_{32} can be designed as $k_{31}(\theta_r - \theta)$ and $k_{32}(\phi_r - \phi)$, correspondingly, where k_{31} and k_{32} are tuning parameters. This is the conventional strategy to reformulate the position control to the speed control.

The initial conditions of the plant are $\theta(0) = 0.2003$, $\phi(0) = 0.4046$, $\dot{\theta}(0) = -1.998$, $\dot{\phi}(0) = -0.0158$, $u_{31}(0) = 0$ and $u_{32}(0) = 0$. The selected control parameters are $N = 50$, $N_u = 2$, $\lambda = 0.0001$, $\alpha = 0.8$, $k_{31} = k_{32} = 10$, and $\omega_{o_{31}} = \omega_{o_{32}} = 5$. The sampling time interval is 2ms. The simulation results are shown in Figs. 9–11. It can be found that although the control law is linear, it is still effective for controlling a switching chaotic system by regulating the control output in a fast manner at the switching instant.

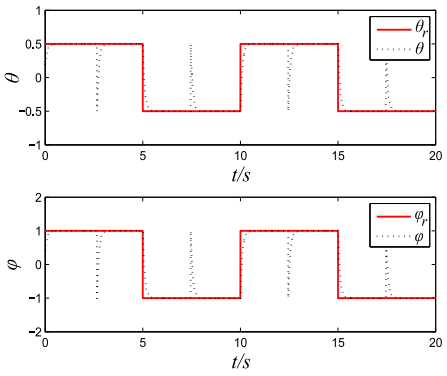

Figure 9. Time responses of θ and ϕ.

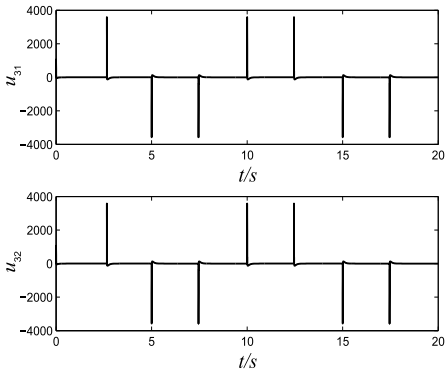

Figure 10. Control outputs.

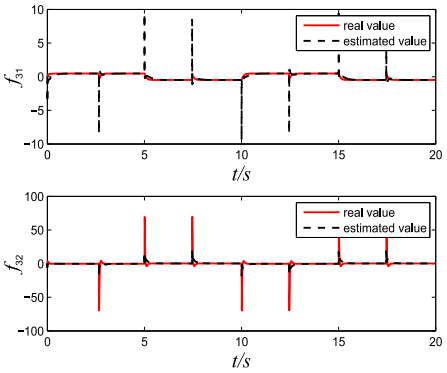

Figure 11. ESO estimations of f_{31} and f_{32}.

5 Conclusion

For the chaotic system, a reduced-order linear extended state observer was utilized to eliminate the nonlinear dynamics so that an integrator could be obtained. Then a unified LTI MPC was proposed for this integrator. Using this method, the sensitivity to precise modeling of chaotic system was reduced, and the future output prediction could be explicitly calculated by only using the current output sample. Thus, the calculation of the Diophantine equation was not required, and the computational complexity was reduced substantially. The effectiveness of the proposed method was verified by the numerical simulations. Therefore, we confirm that a linear time-invariant model predictive controller can be designed in a unified manner to control strong nonlinear chaotic systems.

References

1. S. Boccaletti, C. Grebogi, Y.C. Lai, H. Mancini, D. Maza, The control of chaos: Theory and applications, *Phys. Rep.*, **329**(3):103–197, 2000.
2. T. Botmart, P. Niamsup, X. Liu, Synchronization of non-autonomous chaotic systems with time-varying delay via delayed feedback control, *Commun. Nonlinear Sci. Numer. Simul.*, **17**(4):1894–1907, 2012.
3. D.W. Clarke, C. Mohtadi, P.S. Tuffs, Generalized predictive control—Part I. The basic algorithm, *Automatica*, **23**(2):137–148, 1987.
4. Y. Ding, W. Jiang, H. Wang, Delayed feedback control and bifurcation analysis of Rossler chaotic system, *Nonlinear Dyn.*, **61**(4):707–715, 2010.
5. G. Feng, G. Chen, Adaptive control of discrete-time chaotic systems: A fuzzy control approach, *Chaos Solitons Fractals*, **23**(2):459–467, 2005.
6. Z.Q. Gao, Scaling and bandwidth-parameterization based controller tuning, in *Proceedings of the American Control Conference, Denver, CO, June 4–6, 2003*, IEEE, 2003, pp. 4989–4996.
7. J. Han, From PID to active disturbance rejection control, *IEEE Trans. Ind. Electron.*, **56**(3): 900–906, 2009.

8. S. Kuntanapreeda, *An Observer-Based Neural Network Controller for Chaotic Lorenz System*, Springer, Berlin, Heidelberg, 2008.

9. C.L. Li, L. Wu, H.M. Li, Y.N. Tong, A novel chaotic system and its topological horseshoe, *Nonlinear Anal. Model. Control*, **18**(1):66–77, 2013.

10. Q.D. Li, X.S. Yang, New walking dynamics in the simplest passive bipedal walking model, *Appl. Math. Modelling*, **36**(11):5262–5271, 2012.

11. F.C. Liu, X.M. Liang, A fast algorithm for generalized predictive control and synchronization of Henon chaotic systems, *Acta Phys. Sin.*, **54**(10):4584–4589, 2005.

12. Y. Liu, S. Zhao, J. Lu, A new fuzzy impulsive control of chaotic systems based on T–S fuzzy model, *IEEE Trans. Fuzzy Syst.*, **19**(2):393–398, 2011.

13. A. Luviano-Juárez, J. Cortés-Romero, H. Sira-Ramírez, Synchronization of chaotic oscillators by means of generalized proportional integral observers, *Int. J. Bifurcation Chaos Appl. Sci. Eng.*, **20**(5):1509–1517, 2010.

14. E. Ott, C. Grebogi, J.A. Yorke, Controlling chaos, *Phys. Rev. Lett.*, **64**(5):1196–1199, 1990.

15. K. Pyragas, Delayed feedback control of chaos, *Philos. Trans. R. Soc. Lond., A*, **364**(1864): 2309–2334, 2006.

16. D.M. Qiu, M.W. Sun, Z.H. Wang, Y.K. Wang, Z.Q. Chen, Practical wind-disturbance rejection for large deep space observatory antenna, *IEEE Trans. Control Syst. Technol.*, **22**(5):1983–1990, 2014.

17. Q.M. Shi, L.G. Tang, L. Zhao, A novel chaotic system and its anti-synchronization, in *Proceedings of 2011 Seventh International Conference on Natural Computation, Shanghai, July 26–28, 2011*, IEEE, 2011, pp. 1356–1360.

18. V. Sundarapandian, Adaptive control and synchronization of Liu's four-wing chaotic system with cubic nonlinearity, *Int. J. Comput. Sci. Eng. Appl.*, **1**(4):127–138, 2011.

19. W. Tan, Y.N. Wang, Z.R. Liu, S.W. Zhou, Neural network control for nonlinear chaotic motion, *Acta Phys. Sin.*, **51**(11):2463–2466, 2002.

20. S. Vaidyanathan, Sliding mode controller design for synchronization of Shimizu–Morioka chaotic systems, *Int. J. Inf. Sci. Tech.*, **1**(1):20–29, 2011.

21. U.E. Vincent, Chaos synchronization using active control and backstepping control: A comparative analysis, *Nonlinear Anal. Model. Control*, **13**(2):253–261, 2008.

22. X. Wang, Y. Wang, Adaptive control for synchronization of a four-dimensional chaotic system via a single variable, *Nonlinear Dyn.*, **65**(3):311–316, 2011.

23. Y. Wang, M. Sun, Z. Wang, Z. Liu, Z. Chen, A novel disturbance-observer based friction compensation scheme for ball and plate system, *ISA Trans.*, **53**(2):671–678, 2014.

24. S. Wiggins, S. Wiggins, M. Golubitsky, *Introduction to Applied Nonlinear Dynamical Systems and Chaos*, Springer-Verlag, New York, 1990.

25. Z.G. Wu, P. Shi, H. Su, J. Chu, Sampled-data fuzzy control of chaotic systems based on a T–S fuzzy model, *IEEE Trans. Fuzzy Syst.*, **22**(1):153–163, 2014.

26. M. Yahyazadeh, A.R. Noei, R. Ghaderi, Synchronization of chaotic systems with known and unknown parameters using a modified active sliding mode control, *ISA Trans.*, **50**(2):262–267, 2011.

27. C. Yin, S. Zhong, W. Chen, Design of sliding mode controller for a class of fractional-order chaotic systems, *Commun. Nonlinear Sci. Numer. Simul.*, **17**(1):356–366, 2012.

28. J. Zhang, W. Tang, A novel bounded 4D chaotic system, *Nonlinear Dyn.*, **67**(4):2455–2465, 2012.

29. Q. Zheng, L. Dong, D.H. Lee, Z. Gao, Active disturbance rejection control and implementation for MEMS gyroscope, *IEEE Trans. Control Syst. Technol.*, **17**:1432–1438, 2009.

30. Q. Zheng, F.J. Goforth, An active disturbance rejection based control approach for hysteretic systems, in *Proceedings of the 49th IEEE Conference on Decision and Control, Atlanta, GA, December 15–17, 2010*, IEEE, 2010, pp. 3748–3753.